Macromolecules

Article

pubs.acs.org/Macromolecules

Impact of Solvent Quality on the Hysteresis in the Coil–Stretch Transition of Flexible Polymers in Good Solvents

Rangarajan Radhakrishnan and Patrick T. Underhill*

Department of Chemical and Biological Engineering, Rensselaer Polytechnic Institute, 110 Eighth Street, Troy, New York 12180, United States

Supporting Information

ABSTRACT: Direct observations of long flexible polymers in elongational flow show a coil to stretch transition (CST) and hysteresis in this transition. In this article, solvent effects on the hysteresis of CST were examined using Brownian dynamics simulations of a dumbbell model with conformation dependent drag. A spring force relation that is able to capture the effects of solvent quality was used. Two methods of increasing the solvent quality were analyzed: (1) by increasing the number of Kuhn steps (N_K) and keeping the excluded volume parameter (v/l^3) constant, and (2) by increasing v/l^3 and keeping N_K constant. In the first case, the width of the hysteresis (ratio of upturn to downturn strain rates) increased with increase in N_K. In the second case, the width of hysteresis decreased with increase in v/l^3. This implies that molecules such as ss-DNA, which have $v/l^3 \approx 1$ in good solvents, will have less hysteresis than a molecule with the same N_K in a Θ solvent.

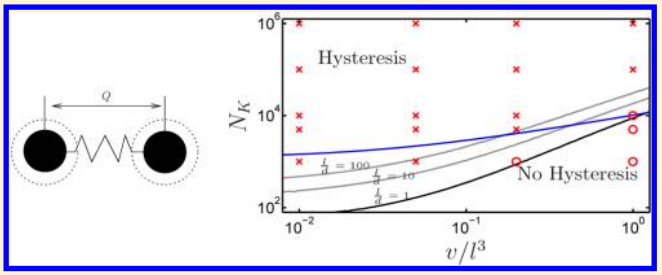

INTRODUCTION

Flow behavior of polymers in dilute solutions have important applications in characterization of polymers,[1,2] in turbulent drag reduction,[3−5] transporting and manipulating DNA in microfludic devices.[6−8] Dilute polymeric solutions are also important to understand from a fundamental standpoint, as a single polymer is an ideal system to study before taking into account interactions with other polymers, particles and surfaces. Brownian Dynamics simulations (BD) using bead spring chain models have been shown to accurately predict the properties of ds-DNA in flow by comparing them with fluorescence experiments.[9,10] ds-DNA served as an ideal polymer to work with, as monodisperse solutions of this molecule could be obtained economically; also, it was known that these molecules behave like ideal worm-like chains.[11] Other long strings of flexible polymers like polystyrene were shown to have different behavior than those predicted from these bead spring models.[2,12] Polystyrene, having greater flexibility than ds-DNA, showed much less deformation under elongational flow than ds-DNA.[12] The solvent–polymer interactions in polystyrene are a possible source for the differences with ds-DNA.[2,12] In this article, the impact of solvent–polymer interactions on the dynamics of flexible polymers in an elongational flow is analyzed.

Elongational flow is generated in many flow devices and can be used for stretching molecules in microfluidic devices. In an elongational flow, long flexible molecules were predicted to undergo a sharp transition from a coiled state to an extended state called the coil–stretch transition (CST).[13,14] Hysteresis in the CST was predicted to occur due to the difference in drag forces between the coiled and extended states of the polymer.[13,14] The CST and its hysteresis were confirmed by direct observation of ds-DNA molecules[15] and indirectly by observation of normal-stress differences of polystyrene in a filament stretching rheometer.[16]

A special condition assuming the ideal behavior of polymers in a solvent is known as the Θ condition.[17] In a Θ condition, the amount of observed hysteresis depends on the length of the molecule. Models and simulations of long polymers were developed to quantify the observed hysteresis in the CST, notably using Brownian dynamics (BD) simulations.[10,18] In these models, the polymer is represented as a chain of beads connected by entropic springs. The hydrodynamic interactions (HI) between the beads were accounted for by means of Rotne–Prager–Yamakawa tensor.[10,18] Hydrodynamic interactions give rise to the difference in the drag coefficients of the fully extended state (ζ^e) and the coiled state (ζ^c), which leads to hysteresis in the CST. Using BD simulations of finitely extensible chains in Θ conditions, it was found that $\zeta^e/\zeta^c \gtrsim 4.5$ was required to observe hysteresis.[18] This criterion closely matches the experimental observations[15] of ds-DNA, which undergoes hysteresis when $\zeta^e/\zeta^c \sim 5$ and no hysteresis when $\zeta^e/\zeta^c \sim 4$. Another common modeling approach to study hysteresis is to use a dumbbell model with conformation dependent drag to represent the polymer.[10,13,14,19−23] The drag coefficient of the beads of the dumbbell is varied with its conformation in order to account for the difference in the drag forces between the coiled and the extended states.

Received: August 29, 2012
Revised: December 13, 2012
Published: December 28, 2012

In good solvent conditions, the effective interactions between the polymer segments are repulsive.[17] A number of experimental and theoretical studies have been performed in good solvents to find the scaling exponent of the critical strain rate with respect to molecular weight in the coil−stretch arm of the CST.[24−31] In contrast, relatively few studies have looked at the impact of solvent quality on the hysteresis in the CST. Using the criterion for drag coefficients to observe hysteresis in Θ solvents ($\zeta^e/\zeta^c \gtrsim 4.5$), Hsieh and Larson[18] calculated that longer molecules with more number of beads than in Θ conditions should be used to observe hysteresis in good solvent conditions. This is because the coil is more swelled, and ζ^e/ζ^c is therefore lower for a molecule with same number of Kuhn steps N_K in good solvents than in Θ solvents.

Recently, Somani et al.[23] carefully studied the solvent effects on the hysteresis using BD simulations. They avoided using large numbers of beads to represent long molecules by extrapolating the results to the limit of using an infinite number of beads while the solvent quality z is held constant. z is given by

$$z = \left(\frac{3}{2\pi}\right)^{3/2} \frac{v}{l^3}\sqrt{N_k} \tag{1}$$

where v/l^3 is the excluded volume parameter. From their extrapolation procedure, for solvent qualities up to $z = 10$, it was found that the coil−stretch arm of the transition is independent of z when the strain rate is scaled by the longest relaxation time.

However, blob theory predicts different responses to external forces for molecules having the same solvent quality z, but having different v/l^3.[32−34] For example, ss-DNA of length $N_K \approx 10^4$ and $v/l^3 \approx 1$ has a nonlinear force extension region known as the Pincus region, without a linear region at higher forces. In contrast, from blob theory, a molecule having the same z but with $v/l^3 \sim 10^{-2}$ and $N_K \approx 10^8$ would have a linear region at higher forces than the Pincus region. Therefore, it is important to understand the influence of both z and v/l^3 on the CST when a significant Pincus region exists. From blob theory, the maximum solvent quality ($z = 10$) used by Somani et al.[23] is not quite large enough to have a significant Pincus region.

In this work, solvent effects on hysteresis are studied by observing molecules with different force extension behaviors. We have previously developed a dumbbell model to account for solvent effects on the force extension of long flexible molecules.[34] Neglecting HI, it was observed that the CST can be modified due to solvent effects. It was found that increasing the numbers of springs representing the polymer did not change the flow results from using the dumbbell model. Therefore, for ease of analysis and computational speed, a dumbbell model with conformation dependent drag is used in this work. We focus our attention on calculating the width and the onset of hysteresis by changing v/l^3 and N_K.

MODEL

The polymer is modeled as a dumbbell as shown in Figure 1. The solvent quality of the polymer is included by means of a spring force relation that can represent polymers from Θ to good solvent.[34] We consider a polymer of N_K number of Kuhn steps, each of length l, and the solvent polymer interactions quantified by an excluded volume v. The spring force acting on the beads separated by a distance Q is taken as

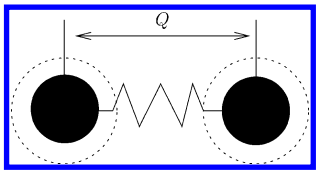

Figure 1. Illustration of a dumbbell model with conformation dependent drag. The dotted circle illustrates the variability of the drag coefficient with extension Q of the dumbbell.

$$F_s(Q) = \frac{AQ^{3/2}}{1 + BQ^{1/2}} \frac{1}{1 - (Q/Q_0)^2} \tag{2}$$

where $Q_0 = N_K l$ is the contour length of the spring.[34] A and B are constants chosen to represent the force extension behavior of molecules in solvent qualities ranging from Θ to good, and are defined as

$$A = \frac{(2.409/\sqrt{z} + 2.122/z)k_B T}{R_\theta^{5/2}} \tag{3}$$

$$B = \frac{2.409/\sqrt{z} + 2.122/z}{3R_\theta^{1/2}} \tag{4}$$

where $R_\theta = N_k^{1/2} l$ is the Θ solvent equilibrium size, k_B is Boltzmann's constant, T is the absolute temperature, and z is given by eq 1.

To include the effect of the variability of the drag on the polymer with its conformation, the drag coefficient ζ was varied based on the extension Q. Different functions for $\zeta(Q)$ have been previously used.[10,13,14,19−23] In order to understand the impact on hysteresis, the key features to include are that $\zeta(Q) \approx$ constant when $Q \sim Q_{Eq}$, and $\zeta \sim Q$ when $Q \gg Q_{Eq}$.[14,19,22,23] Following the work of Tang et al.,[22] $\zeta(Q)$ was taken as

$$\zeta(Q) = \zeta_0(1 + \beta Q) \tag{5}$$

The constants β and ζ_0 are determined from the drag coefficients in equilibrium and fully extended states. The drag coefficient on the bead of a polymer in an extended conformation is calculated by matching the drag on the model to that given by slender body theory for an extended polymer chain[35] as

$$2\zeta(Q = Q_0) \approx \frac{2\pi\eta Q_0}{\log(Q_0/d)} \tag{6}$$

where d is the hydrodynamic diameter of the polymer and η is the viscosity of the fluid. The difference in drag forces in transverse and longitudinal directions from the slender body theory[35] is neglected. This is done because the dominant forces in elongational flow are in the longitudinal direction. In the coiled state, the total drag coefficient for the model is matched to the Stokes' drag on a sphere using the radius of gyration of the polymer (R_g) to approximate the hydrodynamic radius[17] as

$$2\zeta_0 = 2\zeta(Q = 0) \approx 6\pi\eta R_g \tag{7}$$

This estimate of the hydrodynamic radius differs from the renormalization group estimate for polymers in a good solvent only by a constant,[17] and provides the correct qualitative estimate of the drag in the coiled state. After some algebraic manipulations, the constant β for this model is calculated from the ratio of drags in eqs 6 and 7 to be

dx.doi.org/10.1021/ma301815y | Macromolecules 2013, 46, 548−554

$$\frac{\zeta(Q = Q_0)}{\zeta(Q = 0)} = 1 + \beta Q_0 \approx \frac{\sqrt{\frac{2}{3}\frac{R_\theta^2}{\langle Q^2\rangle_{Eq}} N_K}}{(\log(l/d) + \log(N_K))} \quad (8)$$

where $\langle Q^2\rangle_{Eq}$ is evaluated from z using an approximate relation[17,36]

$$\left(\frac{\langle Q^2\rangle_{Eq}}{R_\theta{}^2}\right)^{5/2} - \left(\frac{\langle Q^2\rangle_{Eq}}{R_\theta{}^2}\right)^{3/2} = \frac{4z}{3} \quad (9)$$

As an example, using eqs 8 and 9, ds-DNA with $N_K = 10^4$, $l/d = 100$, and $\nu/l^3 = 0.01$ has a value of $\beta Q_0 \approx 4.2$ and ss-DNA with $N_K = 10^4$, $l/d = 1$, and $\nu/l^3 = 1$ has a value of $\beta Q_0 \approx 3$.

SIMULATION METHODOLOGY

A Brownian dynamics methodology was used to perform the simulations. In Brownian dynamics, a stochastic differential equation for the configuration of the dumbbell neglecting inertia is given as[37]

$$d\mathbf{x}_i = \left(\kappa\cdot\mathbf{x}_i + \frac{\mathbf{D}_{ij}}{k_B T}\mathbf{F}_{s,j} + \frac{\partial}{\partial \mathbf{x}_j}\mathbf{D}_{ij}\right) dt + \sqrt{2}\,\mathbf{B}_{ij}\, d\mathbf{W}_j \quad (10)$$

where $\mathbf{x}_i$ is the position vector of bead i of the dumbbell, $\boldsymbol{\kappa} = \nabla\mathbf{v}^T$ is the transpose of the imposed velocity gradient tensor, $\mathbf{F}_{s,j}$ is the spring force acting on the bead j, and summation over the repeated index j is implied. $d\mathbf{W}_j$ is a random vector for which each component has zero mean and variance dt. The tensors $\mathbf{D}_{ij}$ and $\mathbf{B}_{ij}$ are 3×3 blocks of the larger $\mathbf{D}$ and $\mathbf{B}$ tensors. Because direct hydrodynamic interactions are not included between the beads, the diffusion tensor $\mathbf{D}_{ij}$ is given by

$$\mathbf{D}_{ij} = \frac{k_B T}{\zeta(Q)}\delta_{ij} I \quad (11)$$

where I is the identity tensor, δ_{ij} is the Kronecker delta, and $\zeta(Q)$ is the bead drag coefficient given by eq 5. The divergence of $\mathbf{D}_{ij}$ is computed analytically using the definition $\mathbf{Q} = \mathbf{x}_2 - \mathbf{x}_1$, since $\zeta(Q)$ is a simple function. In order to satisfy the fluctuation dissipation relation, the tensor $\mathbf{B}$ must obey the condition $\mathbf{B}\cdot\mathbf{B}^T = \mathbf{D}$. Since $\mathbf{D}$ is diagonal in our model, $\mathbf{B}$ is also diagonal and equal to the square root of $\mathbf{D}$. Equation 10 is integrated by stepping forward in time by a first order Eulerian scheme of integration.[38]

Simulations are performed in uniaxial elongational flow at a range of elongation rates. The extensional axis is taken to be the z-axis, and therefore κ is equal to

$$\boldsymbol{\kappa} = \begin{pmatrix} -\dot{\varepsilon}/2 & 0 & 0 \\ 0 & -\dot{\varepsilon}/2 & 0 \\ 0 & 0 & \dot{\varepsilon} \end{pmatrix} \quad (12)$$

where $\dot{\varepsilon}$ is the elongation rate. To capture the hysteresis of the CST from BD simulations, two sets of simulations of a single dumbbell are performed. Below and above the hysteresis region, both simulations give the same result. In the hysteresis region, two metastable states exist separated by a free energy barrier. The average over the course of a simulation will then depend on the starting configuration and the amount of hopping between states over the course of the simulation. Our goal is to calculate the averages within those two states. The two sets of simulations begin with $Q = 10^{-4}Q_0$ and $Q = 0.95Q_0$ in order to calculate the lower and upper branches, respectively. The system is simulated in flow for at least 250 longest relaxation times before any data is collected. Below the transition, data is collected for at least 900 longest relaxation times. Above the transition, data is collected for at least 450 Hencky strain units. Once data is collected, averages are computed separately for each of the two metastable states, where we choose $Q^2 = 0.1Q_0{}^2$ as the border between the two states. Calculations were also done with $Q^2 = 0.01Q_0{}^2$, and they did not give different results.

All the strain rates are scaled by the longest relaxation time λ found by fitting BD simulations of extended molecules ($Q = 0.9Q_0$) relaxing toward equilibrium. A nonlinear fit of $\langle Q^2\rangle - \langle Q^2\rangle_{Eq}$ near equilibrium to $\exp(-t/\lambda)$ was used to calculate λ (not shown).

Force Balance Theory. Away from equilibrium the fluctuations are negligible and the steady state elongational flow response of the molecule can be predicted by a balance of forces along the axis of extension.[23,34,39] The forces acting on each bead of the dumbbell along the axis of extension are the spring force F_s and the drag force F_d, whose balance is given by

$$F_d = F_s \quad (13)$$

The spring force F_s is given by eq 2 and the drag force acting on a bead of the dumbbell F_d is

$$F_d = \frac{\zeta(Q)\dot{\varepsilon}Q}{2} \quad (14)$$

For each molecule and elongation rate, eq 13 can be solved for the extension Q. Since this theory is not valid at equilibrium (when fluctuations are important), the theory can predict an extension smaller than the equilibrium value. If this occurs, we set the prediction from the theory equal to the equilibrium size. At some elongation rates, multiple solutions exist, corresponding to hysteresis. Figure 2 shows the intersection of the spring and drag forces for a molecule of $N_K = 10^6$ and $\nu/l^3 = 0.2$ at an elongation rate for which hysteresis occurs. The points of intersection between the drag force (dashed line) and the spring force (solid line) in Figure 2 correspond to the solutions of the force balance theory. It can be seen from Figure 2 that there are two stable solutions between the dashed and solid lines, and an unstable solution in the middle. On the basis of the initial configuration, a molecule can be in either of these

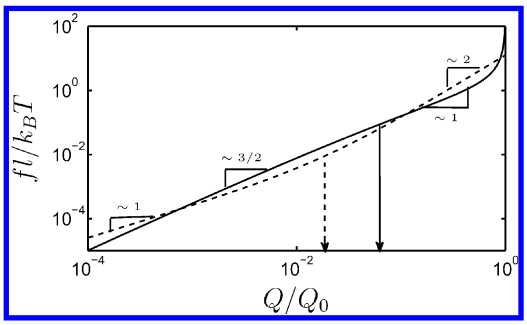

Figure 2. The force balance picture is illustrated for a molecule of $\nu/l^3 = 0.2$ and $N_K = 10^6$. The solid line indicates the spring force and the dashed line indicates the drag force. Approximate power law exponents n of the forces $f \sim Q^n$ in different regions are noted. The approximate transition point between the scaling regions in drag force is indicated by a dashed arrow at an extension of $Q = 1/\beta$ and that of the spring force is indicated by a solid arrow at an extension of $Q = Q_0\nu/(3l^3)$.

dx.doi.org/10.1021/ma301815y | Macromolecules 2013, 46, 548−554

stable solutions. The existence of two stable solutions gives rise to the phenomena of conformational hysteresis in the CST.

These solutions, and hysteresis, arise due to the different power law scaling exponents of the spring and drag forces. The drag force is $F_d \sim Q$ when $Q < 1/\beta$ and $F_d \sim Q^2$ when $Q > 1/\beta$. The spring force is $F_s \sim Q^{3/2}$ when $Q < Q_0\nu/(3l^3)$ and $F_s \sim Q$ when $Q_0\nu/(3l^3) < Q < Q_0/3$. These scaling estimates can be used to approximate the numerical solution to eq 13.

RESULTS

Polymer solvent interactions lead to differences in the elasticity or the resistance to stretching of a molecule.[32−34,40] These differences in force−extension (FE) behavior lead to differences in the flow behavior of the molecules. In this work, the dumbbell model is used to investigate differences in hysteresis and in the nature of the CST between different molecules. The parameters ν/l^3, N_K, and aspect ratio l/d were treated independently as there exists no simple relation between them for different molecules of same contour length and different salt concentrations.[33] The present study is undertaken to understand the importance of each of these parameters in determining the width of hysteresis in the CST. In experiments comparing molecules, changes in solvent conditions or molecular structure that change the excluded volume parameter ν/l^3 could also change the number of Kuhn steps N_K and the aspect ratio l/d.

BD Simulations without HI. To understand the role of HI in determining the CST, it is useful to first observe the response of the same molecules when HI is neglected. The FE and the CST depend on ν/l^3 and N_K of a molecule.[34] When HI is neglected, the FE curve determines the flow response. To analyze the impact of ν/l^3 on the FE and consequently the CST, molecules with the same number of Kuhn steps $N_K = 10^4$, but with ν/l^3 of 0.01, 0.2, and 1 are considered.

In Figure 3a, the average extension $\langle Q_z\rangle$ in the direction of applied force f of the three different molecules from BD simulations of our model are shown. Increasing ν/l^3 increases the solvent quality z, which gives rise to the Pincus region of $\langle Q_z\rangle \sim f^{2/3}$ in the FE.[34] Figure 3b shows the response in flow neglecting HI ($\zeta(Q) = \zeta_0$) and a comparison to the solution from the force balance theory. The Weissenberg number Wi = $\dot{\epsilon}\lambda$ characterizes the strength of flow, where λ is the longest relaxation time.

Note that only the first three regions of the FE curve are affected by solvent effects, and the high force region in the FE curve of ds-DNA, ss-DNA are different from that of eq 2. Therefore, the high strain rate response of the molecules are not captured by the current model. Further details of the model and its analysis without HI can be found in ref 34.

BD Simulations of Dumbbell Model with Variable Drag Coefficient. In this section, the impact of solvent quality on the elongational flow response of polymers is examined using the model with variable drag coefficient described earlier. The response of the three molecules of $N_K = 10^4$ and $\nu/l^3 =$ 0.01, 0.2, and 1 are examined. They have different z and FE behaviors (as seen in Figure 3) but also different β, which is calculated from eq 8. For ease of analysis, we neglect the dependence of β on l/d by assuming that $l/d = 1$ for all the molecules under consideration. To allow for differences in the estimates of β, the response of the molecules if βQ_0 were changed by ±30% are shown in the Supporting Information. Later in this section, the effect of increasing N_K of these molecules is considered.

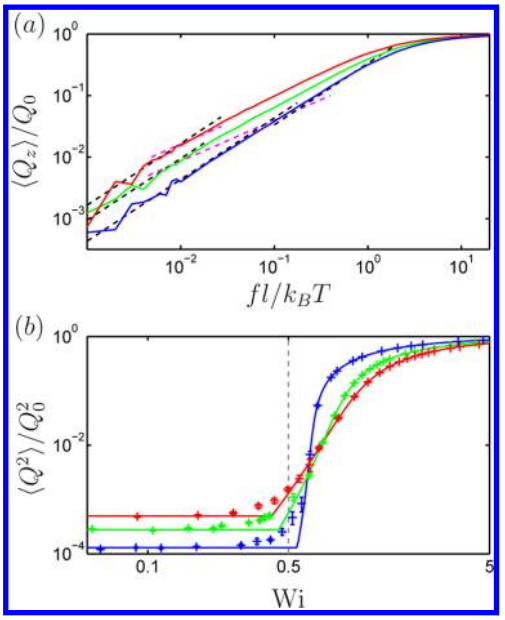

Figure 3. BD simulations of force−extension and elongational flow behavior without conformation dependent drag. (a) Force−extension behavior of the dumbbell model of a molecule of length $N_k = 10^4$ and different solvent conditions: $\nu/l^3 = 0.01$ (blue line), $\nu/l^3 = 0.2$ (green line), and $\nu/l^3 = 1$ (red line). The black dashed line represents the linear region and the magenta dashed line represents the $Q_z \sim f^{2/3}$ scaling. (b) Stretch of these molecules in elongational flow without including conformation dependent drag. Results of BD simulations (+) of molecules of $N_k = 10^4$ and $\nu/l^3 = 0.01$ (blue), $\nu/l^3 = 0.2$ (green) and $\nu/l^3 = 1$ (red). The lines in the same colors represent the force balance theory. The gray dashed line represents a Wi = 0.5.

First, the impact of excluded volume parameter ν/l^3 in determining the width of hysteresis for molecules of $N_K = 10^4$ is examined. In Figure 4a, the response with $\nu/l^3 = 0.01$ is shown. The flow response shows hysteresis in the CST. The parameters of our model are similar to that of ds-DNA experiments .[15] $\beta Q_0 = 6.605$ calculated for this case is greater than the estimate of $\beta Q_0 \approx 5$ for ds-DNA of $N_K \approx 9280$ from experiments[15] which show hysteresis in the CST. This is because our estimate does not include contribution of ln l/d for ds-DNA in eq 8. For ds-DNA of $l/d = 50$, $\beta Q_0 \approx 4.46$ shows a slightly lower value for the width of hysteresis, and is near the lower value shown in the Supporting Information. In Figure 4b, the response of our model with $\nu/l^3 = 0.2$ also shows hysteresis in the CST. However, the width of hysteresis is less than that of the previous case. The reason for the decrease in the width of the hysteresis loop is that the molecule is more swelled in the coiled state and therefore the value computed for $\beta Q_0 = 4.141$ is less than the previous case. Conformation-dependent drag also sharpens the transition compared to the one in Figure 3. Note that PEG in good solvents was determined to have a similar $\nu/l^3 \approx 0.2$.[41] In Figure 4c, the response of a molecule with $\nu/l^3 = 1$ is shown. This model is comparable to ss-DNA.[34] The flow response for this case does not show hysteresis. Again, the ratio of drags between the extended and coiled state is less compared to the previous cases due to more swelling in the coiled state and a $\beta Q_0 = 2.886$ is calculated. From Figure 4 we observe that with increasing excluded volume parameter ν/l^3, the width of hysteresis decreases.

Second, in Figure 5 the effect of increasing the number of Kuhn steps ($N_K = 10^4$, 10^5, and 10^6) for different excluded volume parameters ($\nu/l^3 = 0.01$, $\nu/l^3 = 0.2$, and $\nu/l^3 = 1$) are

dx.doi.org/10.1021/ma301815y | Macromolecules 2013, 46, 548−554

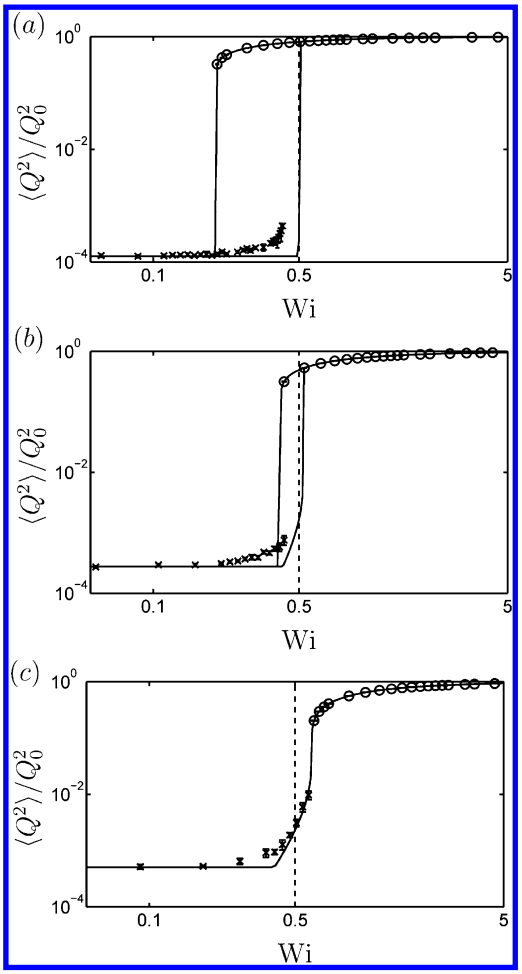

Figure 4. BD simulations of elongational flow behavior of a molecule in different solvent conditions. The figures show the elongational flow behavior of the molecule of length $N_k = 10^4$ and (a) with $\nu/l^3 = 0.01$ and (b) with $\nu/l^3 = 0.2$ and (*c*) with $\nu/l^3 = 1$. BD simulations of the upturn in the CST is given by the × symbol and the downturn is given by ○. The solid lines represent the solution from the force balance theory. The dashed line of Wi = 0.5 is shown here for reference.

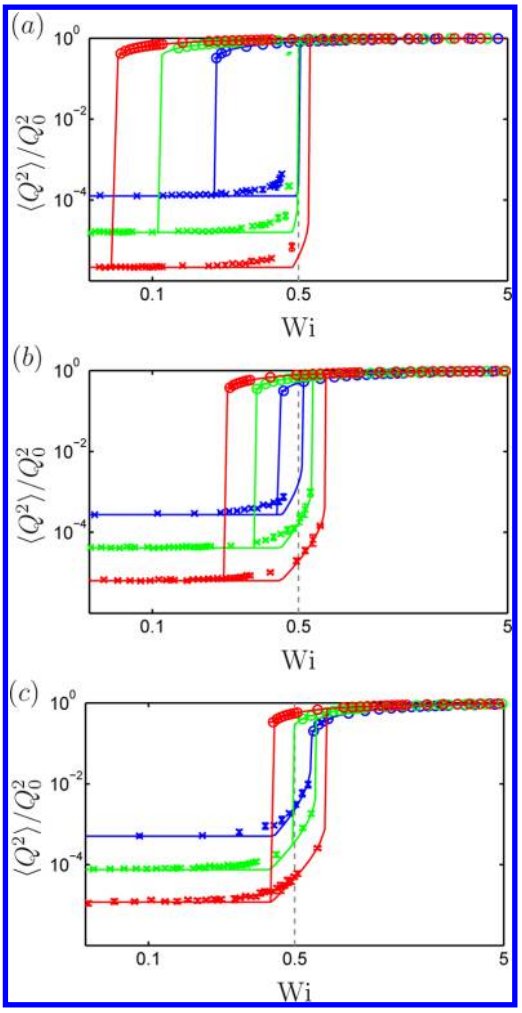

Figure 5. BD simulations of elongational flow behavior of molecules of different N_K and ν/l^3. Each subfigure has a different ν/l^3: (*a*) $\nu/l^3 = 0.01$, (*b*) $\nu/l^3 = 0.2$, and (*c*) $\nu/l^3 = 1$. Each color represents molecules of the same N_K: $N_k = 10^4$ (blue), $N_k = 10^5$ (green), and $N_k = 10^6$ (red). The symbols represent the results of BD simulations, with × representing the upturn and ○ representing the downturn arm of the CST. The solid lines represent the solution from the force balance theory. The dashed line of Wi = 0.5 is shown in gray for reference.

examined. The width of hysteresis increases with increase in N_K. The critical Wi for the upturn from the simulations and the force balance solution ranges from 0.5 to 0.75. Also, note that the molecules with larger ν/l^3 are partially stretched due to the $Q \sim f^{2/3}$ in FE before the upturn of the CST. It is again clear that with molecules of same N_K, hysteresis decreases with increasing ν/l^3. The width of hysteresis and the minimum N_K for the onset of hysteresis are quantified in the next section. These results agree well with the prediction by Hsieh and Larson[18] that longer molecules are needed to observe hysteresis of the CST in good solvents.

The results of this work show differences from the previous study by Somani et al.[23] From Brownian dynamics simulations using few springs and by extrapolation to an infinite number of springs, Somani find that the upturn in the CST is dependent on solvent quality. The critical Wi is found to be a constant which seems to agree with our results. However, they find that the width of hysteresis in the CST is invariant, increasing or decreasing based on how the strain rates are scaled. This conclusion is incorrect even based on their data. It is known that the downturn in the CST is independent of solvent quality, and upturn is dependent on solvent quality as mentioned previously. In contrast to their claim, it is clear that the width of the hysteresis depends on solvent quality and cannot be modified based the scaling of strain rates. Further, it is found that the width of hysteresis in the CST depends not only *z*, but on both N_K and ν/l^3. It should be noted that the high strain rate response of different molecules will slightly alter the value of the width of hysteresis due to the differences in their high force FE response.

The BD simulations have shown how the presence and amount of hysteresis depends on N_K and ν/l^3 in good solvents. The force balance theory matches the simulations almost quantitatively. It is useful to combine these simulations and theory into a general picture of the CST. Assuming that the spring and drag forces have sharp transitions between the different regions in *Q* and that all regions are wide, we can develop a "scaling picture" of the transition points and amount of hysteresis.

This scaling picture is shown in Figure 6. The black line represents the scaling response when $\beta = 0$. This is the response until $\beta Q_0 \approx 3$, above which there is hysteresis. When

dx.doi.org/10.1021/ma301815y | *Macromolecules* 2013, 46, 548−554

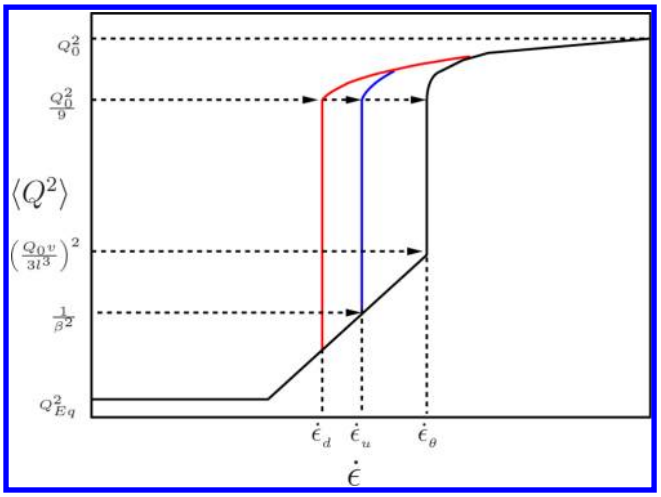

Figure 6. Scaling picture of elongational flow behavior of a molecule with conformation dependent drag. The different possible regions of the flow behavior are illustrated in this figure. The black solid line is the result without conformation dependent drag. The blue and red solid lines indicate the upturn and the downturn arms of the CST respectively.

$\beta Q_0 \lesssim 3$, the four different regions of the force−extension (FE) of a molecule give rise to the four different scaling regions in the flow response. The crossover point between regions 2 and 3 of the FE is at $Q \sim v/l^3 \times Q_0/3$, which determines the end of $Q \sim \dot{\epsilon}^4$ region. $Q \sim Q_0/3$ approximately determines the crossover of the FE into the high force region. This response is the same as noted in our previous article.[34] Note that the criterion for hysteresis is comparable to $\zeta^e/\zeta^c \gtrsim 4.5$ to observe hysteresis predicted by previous works,[15,18] which from eq 8 can be rewritten as $\beta Q_0 \gtrsim 3.5$.

When $\beta Q_0 \gtrsim 3$, the drag coefficient in eq 5 becomes nonlinear when $Q \sim 1/\beta$. This gives an approximate value for the upper critical transition point $\dot{\epsilon}_u$. At $\dot{\epsilon}_u$, $F_d \sim Q^2$ compared to $F_s \sim Q^{3/2}$, which results in a sharp CST until the spring is in the finitely extensible region. This is illustrated by the blue curve in Figure 6.

The maximum value of the transition strain rate occurs when βQ_0 is smaller than the critical value and is equal to the Θ solvent transition point $\dot{\epsilon}_\theta$. This transition happens at Wi = 1/2 based on the Θ solvent longest relaxation time. The critical transition point of the stretch to coil arm of the transition $\dot{\epsilon}_d$ can be estimated by calculating the minimum strain rate until which an extension of $Q = Q_0/3$ is stable. This is illustrated in the flow curve of Figure 6 by a solid red curve.

Solvent Effects on the Onset and Width of Hysteresis. In this section, the onset and width of conformational hysteresis under different solvent conditions are quantified. In Figure 7, symbols denote when hysteresis does and does not occur in the BD simulations. The force balance theory accurately predicts the boundary of the onset of hysteresis and its dependence on N_K and v/l^3. For comparison, the criterion $\beta Q_0 \gtrsim 3$ from eq 8 is shown. Although it has the same trends with N_K and v/l^3, it does not quantitatively match the BD simulations. Since the force balance theory accurately predicts the boundary of the onset of hysteresis for molecules with $l/d = 1$, only the force balance theory is shown for $l/d = 10$ and $l/d = 100$.

The width of hysteresis (W_H) is defined as

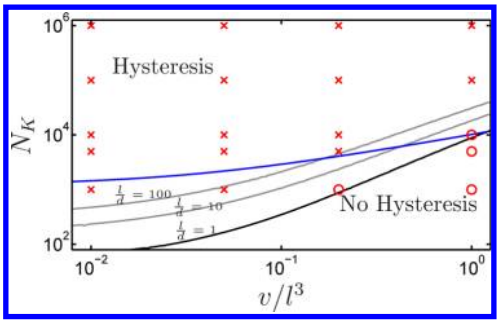

Figure 7. "Phase-plot" of N_k vs v/l^3 for the onset of hysteresis for a dumbbell model. The symbol × represent molecules with hysteresis and the symbol ○ represent molecules with no hysteresis, from the results of Brownian dynamics simulations of these molecules with $l/d = 1$. The solid black line is the numerical solution of the force-balance predicting the onset of hysteresis for aspect ratio $l/d = 1$. The gray lines are the numerical solutions of force-balance lines for the onset of hysteresis for $l/d = 10$ and $l/d = 100$. The solid blue line represents $\beta Q_0 = 3$ for $l/d = 1$.

$$W_H = \frac{\dot{\epsilon}_u}{\dot{\epsilon}_d} \tag{15}$$

where $\dot{\epsilon}_u$ is the upper critical transition point and $\dot{\epsilon}_d$ is the lower critical transition point. Hysteresis occurs when $W_H > 1$.

The effect of increasing the length of the molecule at a given v/l^3 on the width of hysteresis W_H is shown in Figure 8. The

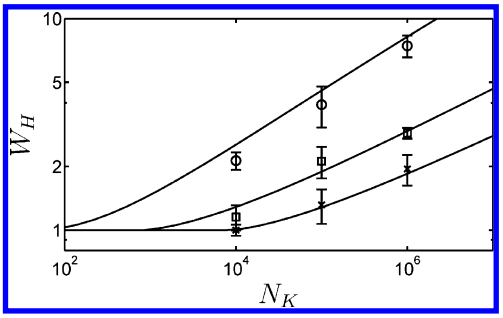

Figure 8. Width of hysteresis W_H is plotted for increasing N_K. The symbol × represents a molecule of $v/l^3 = 1$, □ indicates a $v/l^3 = 0.2$ and ○ indicates a $v/l^3 = 0.01$. The solid lines are the numerical solutions from the force-balance for the width of hysteresis.

results of BD simulations of the 3 previously considered molecules of $v/l^3 = 0.01$, 0.2, and 1 are compared against that of the force-balance theory. The error bars in W_H from the BD simulations are due to the errors in finding the exact value of strain rates $\dot{\epsilon}_u$ and $\dot{\epsilon}_d$ of the CST. The relative error in W_H was calculated by adding the relative errors of obtaining $\dot{\epsilon}_u$ and $\dot{\epsilon}_d$ from the range of $\dot{\epsilon}$ simulated.

The width of the hysteresis from BD simulations is predicted well by the numerical solution of the force balance theory. This quantifies the trend in the width of hysteresis observed with increase in N_K and v/l^3. The width of hysteresis increases with increase in N_K at a given v/l^3. For molecules with the same N_K, those with larger v/l^3 have less hysteresis.

CONCLUSIONS

BD simulations and force balance theory were used to understand the impact of solvent quality in long flexible molecules. Using a dumbbell model to represent the polymer we find that solvent effects impact the hysteresis in the CST.

dx.doi.org/10.1021/ma301815y | Macromolecules 2013, 46, 548−554

Different ways of increasing the solvent quality affect the width of hysteresis differently. If the number of Kuhn steps N_K is held constant and v/l^3 increased, the width of hysteresis decreases. If the number of Kuhn steps N_K is increased, the width of hysteresis increases. We have found using this model that hysteresis can be eliminated for some molecules by increasing the solvent quality at a given N_K. Future experiments need to be performed to test the accuracy of our model.

■ ASSOCIATED CONTENT

Supporting Information

Flow behavior of dumbbell model with different estimates of βQ_0. This material is available free of charge via the Internet at http://pubs.acs.org.

■ AUTHOR INFORMATION

Corresponding Author

*E-mail: underhill@rpi.edu.

Notes

The authors declare no competing financial interest.

■ ACKNOWLEDGMENTS

We gratefully acknowledge support by NSF Grant No. CBET-0954445.

■ REFERENCES

(1) Vlassopoulos, D.; Schowalter, W. R. *J. Rheol.* **1994**, *38*, 1427−1446.
(2) Larson, R. G. *J. Rheol.* **2005**, *49*, 1−70.
(3) Virk, P. S. *AIChE J.* **1975**, *21*, 625−656.
(4) White, C. M.; Mungal, M. G. *Annu. Rev. Fluid Mech.* **2008**, *40*, 235−256.
(5) Dimitropoulos, C. D.; Dubief, Y.; Shaqfeh, E.; Moin, P.; Lele, S. K. *Phys. Fluids* **2005**, *17*, 011705.
(6) Shaqfeh, E. S. G. *J. Non-Newtonian Fluid Mech.* **2005**, *130*, 1−28.
(7) Randall, G. C.; Schultz, K. M.; Doyle, P. S. *Lab Chip* **2006**, *6*, 516−525.
(8) Hsieh, C. C.; Balducci, A.; Doyle, P. S. *Macromolecules* **2007**, *40*, 5196−5205.
(9) Hur, J. S.; Shaqfeh, E. S. G.; Babcock, H. P.; Smith, D. E.; Chu, S. *J. Rheol.* **2001**, *45*, 421−450.
(10) Schroeder, C. M.; Shaqfeh, E. S. G.; Chu, S. *Macromolecules* **2004**, *37*, 9242−9256.
(11) Marko, J. F.; Siggia, E. D. *Macromolecules* **1995**, *28*, 8759−8770.
(12) Li, L.; Larson, R. G.; Sridhar, T. *J. Rheol.* **2000**, *44*, 291−322.
(13) De Gennes, P. G. *J. Chem. Phys.* **1974**, *60*, 5030−5042.
(14) Hinch, E. J. *Phys. Fluids* **1977**, *20*, S22−S30.
(15) Schroeder, C. M.; Babcock, H. P.; Shaqfeh, E. S. G.; Chu, S. *Science* **2003**, *301*, 1515−1519.
(16) Sridhar, T.; Nguyen, D. A.; Prabhakar, R.; Prakash, J. R. *Phys. Rev. Lett.* **2007**, *98*, 167801.
(17) Doi, M.; Edwards, S. F. *The Theory of Polymer Dynamics*; Oxford University Press: New York, 1988.
(18) Hsieh, C.-C.; Larson, R. G. *J. Rheol.* **2005**, *49*, 1081−1089.
(19) Fuller, G. G.; Leal, L. G. *J. Non-Newtonian Fluid Mech.* **1981**, *8*, 271−310.
(20) Brestkin, Y. V.; Gotlib, Y. Y.; Klushin, L. I. *Polymer Science U.S.S.R.* **1989**, *31*, 1249−1256.
(21) Darinskii, A. A.; Lyulin, A. V.; Saphiannikova, M. G. *Int. J. Polym. Mater.* **1993**, *22*, 15−24.
(22) Tang, J.; Trahan, D. W.; Doyle, P. S. *Macromolecules* **2010**, *43*, 3081−3089.
(23) Somani, S.; Shaqfeh, E. S. G.; Prakash, J. R. *Macromolecules* **2010**, *43*, 10679−10691.
(24) Rabin, Y.; Henyey, F. S.; Pathria, R. K. *Phys. Rev. Lett.* **1985**, *55*, 201−203.
(25) Brestkin, Y. V.; Saddlkov, I. S.; Agranova, S. A.; Baranov, V. G.; Frenkel, S. *Polym. Bull.* **1986**, *15*, 147−151.
(26) Narh, K. A.; Odell, J. A.; Keller, A. *J. Polym. Sci., Part B: Polym. Phys.* **1992**, *30*, 335−340.
(27) Menasveta, M. J.; Hoagland, D. A. *Macromolecules* **1992**, *25*, 7060−7062.
(28) Nguyen, T. Q.; Yu, G.; Kausch, H. H. *Macromolecules* **1995**, *28*, 4851−4860.
(29) Cifre, J. G. H.; de la Torre, J. G. *J. Rheol.* **1999**, *43*, 339−358.
(30) Andrews, N. C.; Doufas, A. K.; McHugh, A. J. *Macromolecules* **1998**, *31*, 3104−3108.
(31) Pelletier, E.; Viebke, C.; Meadows, J.; Williams, P. A. *Langmuir* **2003**, *19*, 559−565.
(32) Saleh, O. A.; McIntosh, D. B.; Pincus, P.; Ribeck, N. *Phys. Rev. Lett.* **2009**, *102*, 68301.
(33) McIntosh, D. B.; Ribeck, N.; Saleh, O. A. *Phys. Rev. E* **2009**, *80*, 41803.
(34) Radhakrishnan, R.; Underhill, P. T. *Soft Matter* **2012**, *8*, 6991−7003.
(35) Batchelor, G. K. *J. Fluid Mech.* **1970**, *44*, 419−440.
(36) Yamakawa, H. *Modern theory of polymer solutions*; Harper & Row: New York, 1971.
(37) Jendrejack, R. M.; De Pablo, J. J.; Graham, M. D. *J. Chem. Phys.* **2002**, *116*, 7752−7759.
(38) Grassia, P. S.; Hinch, E. J.; Nitsche, L. C. *J. Fluid Mech.* **1995**, *282*, 373−403.
(39) Bird, R. B.; Armstrong, R. C.; Hassager, O.; Curtiss, C. F. *Dynamics of Polymeric Liquids*; Wiley: New York, 1987; Vol. 2.
(40) Pincus, P. *Macromolecules* **1976**, *9*, 386−388.
(41) Dittmore, A.; McIntosh, D. B.; Halliday, S.; Saleh, O. A. *Phys. Rev. Lett.* **2011**, *107*, 148301.